HOKKAIDO UNIVERSITY

Title	Derivation of deformation characteristics in fast-moving glaciers
Author(s)	Herzfeld, Ute C.; Clarke, Garry K. C.; Mayer, Helmut; Greve, Ralf
Citation	Computers & Geosciences, 30(3), 291-302 https://doi.org/10.1016/j.cageo.2003.10.012
Issue Date	2004-04
Doc URL	http://hdl.handle.net/2115/34679
Type	article (author version)
File Information	Herzfeld_etal_2004_CompGeosci.pdf

Instructions for use

Hokkaido University Collection of Scholarly and Academic Papers : HUSCAP

Computers & Geosciences **30** (3), 291–302, 2004
http://www.elsevier.com/locate/cageo
— Authors' final version —

Derivation of deformation characteristics in fast-moving glaciers

Ute C. Herzfeld (1,2), Garry K. C. Clarke (3),
Helmut Mayer (4) and Ralf Greve (4,5)

(1) Cooperative Institute for Research in Environmental Sciences /
National Snow and Ice Data Center,
University of Colorado, Boulder, CO 80309-0449, USA

(2) Geomathematik, Universität Trier,
D-54286 Trier, Germany

(3) Department of Earth and Ocean Sciences,
University of British Columbia, Vancouver, BC, Canada V6T 1Z4

(4) Fachbereich Mechanik, Technische Universität Darmstadt,
D-64289 Darmstadt, Germany

(5) Institute of Low Temperature Science, Hokkaido University,
Sapporo 060-0819, Japan

January 15, 2004

Correspondence to: U.C. Herzfeld (herzfeld@tryfan.colorado.edu)

Abstract

Crevasse patterns are the writings in a glacier's history book – the movement, strain and deformation frozen in ice. Therefore by analysis of crevasse patterns we can learn about the ice-dynamic processes which the glacier has experienced. Direct measurement of ice movement and deformation is time-consuming and costly, in particular for large glaciers; typically, observations are lacking when sudden changes occur. Analysis of crevasse patterns provides a means to reconstruct past and ongoing deformation processes mathematically. This is especially important for fast-moving ice.

Ice movement and deformation are commonly described and analyzed using continuum mechanics and measurements of ice velocities or strain rates. Here, we present a different approach to the study of ice deformation based on principles of structural geology. Fast ice movement manifests itself in the occurrence of crevasses. Because crevasses remain after the deformation event and may be transported, overprinted or closed, their analysis based on aerial videography and photography or satellite data gives information on past deformation events and resulting strain states. In our treatment, we distinguish (A) continuously fast-moving glaciers and ice streams, and (B) surge-type glaciers, based on observations of two prototypes, Jakobshavns Isbræ, Greenland, for (A), and Bering Glacier, Alaska, during the 1993-1995 surge, for (B).

Classes of ice-deformation types are derived from aerial images of ice surfaces using structural geology, i.e. structural glaciology. For each type, the deformation gradient matrix is formed. Relationships between invariants used in structural geology and continuum mechanics and the singular value decomposition are established and applied to ice-surface classification.

Deformation during a surge is mostly one of the extensional deformation types. Continuously, or infinitesimally repeated, deformation acting in continuously fast-moving ice causes different typical crevasse patterns. The structural-geology approach also includes a way to treat the problem of shear, as observed in the margins of fast-moving ice streams within slow-moving surrounding ice. In this paper we provide the first link between a physical analysis of ice-surface deformation and a connectionist-geostatistical analysis of the same problem.

1 Introduction

Fast-moving glaciers are relatively rare but important. Fast-moving outlet glaciers of the Greenland and Antarctic Ice Sheets play a key role in any scenario of a possible break-up of the ice sheets, as is predicted by some ice-sheet models as a consequence of

global warming. Rapidly accelerating ice during a glacier surge causes an environmental catastrophe. The phenomenon of fast-moving ice still presents unanswered questions to glaciologists. Therefore, it is important to utilize any type of data that may aid in the investigation of fast-moving ice.

In slow-moving ice, such as in most alpine glaciers (typical velocity is 30 m/yr), ductile deformation prevails. Only at specific locations the elasticity threshold is exceeded, brittle failure occurs, and crevasses form (e.g. at the bergschrund, at the lateral margins, at steep sections, at rock protrusions, or at the front). The dynamics of fast-moving glaciers are much less well understood but manifest themselves in the formation of crevasses (brittle deformation, cracks in the continuum). Previous studies of crevasses have been contributed, for example, by Vornberger and Whillans (1990) and Rist et al. (1999), while an example of structural-geological strain analysis of glaciers is found in Marmo and Wilson (1998), for instance.

In this paper, we explore an approach that utilizes crevasse patterns as a source of geophysical or glaciological information. In a practical example, the analysis of crevasse patterns proceeds by (1) determination of crevasse classes using structural geology (e.g., Fig. 1), and (2) determination of a deformation type for each observation (e.g., an image of the crevassed surface) by association of a crevasse class using a neural network (connectionist-geostatistical method, Herzfeld and Zahner, 2001, see Section 6). The most studied variable in ice dynamics in the literature is ice velocity.

Commonly, glaciologists utilize the strain rate tensor to investigate ice deformation. The strain rate tensor is the symmetric part of the velocity gradient tensor, which is the Jakobi matrix of the velocity field. This restriction to symmetric matrices, however, leads to ambiguities in the study of deformation; not all classes can be resolved (for instance, shear and two-directional extension would fall in the same class; cf. Fig. 1). Instead, we use the deformation gradient matrix (see Section 5).

Structural geology has seen a variety of approaches. The presentation in Ramsay and Lisle (2000) was selected as starting point for the transfer of methods from structural geology, because it uses linear algebra and a tie to continuum mechanics. Other presentations are given by Means (1976), Sanderson (1982), Suppe (1985) and Twiss and Moores (1992), among others. Terminology is fraught with difficulties in structural geology and therefore always a subject of debate. Although it may be desirable in principle to use different terms for stress and strain features (see, e.g., Marrett and Peacock, 1999), all such proposals to date have created some linguistically erroneous or unaesthetic terms (such as "contraction" or "shortening" as a strain term for compression) (cf. Şengör, 2002). Here, we use extension and compression for both strain and stress features, as it is always clear from the context which is meant.

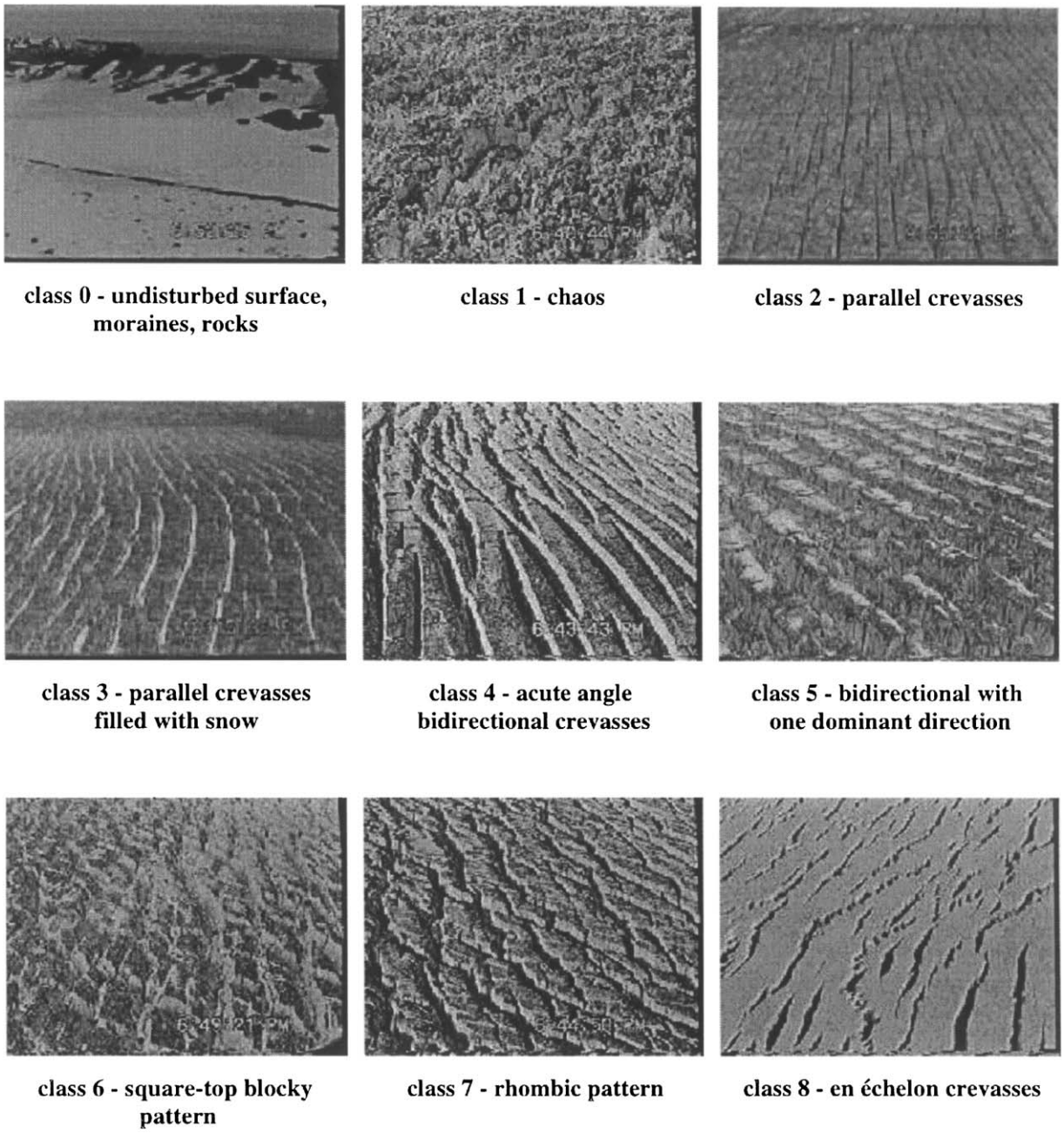

Figure 1: Typical classes of crevasse patterns from video images of Bering Glacier, Alaska.

Analysis of crevasse patterns opens a possibility for study of events that one noticed after they have occurred. Examples are plentiful, because many glaciers are located in remote regions, but the events may be significant indicators of dynamic or climatic change and sources of sea-level rise.

2 Types of fast-moving ice

Following Clarke (1987) we distinguish types of fast-moving ice: (a) fast-moving ice streams, (b) surge-type glaciers, and the special case of (c) Antarctic ice streams (which are absolutely much slower than fast-moving ice streams, but faster than the surrounding ice, with dynamics similar to fast-moving ice streams). We build on this classification and refine it in a way that differences in mathematical treatment become apparent.

(A') Continuously fast-moving glaciers and ice streams.

(B') Surge-type glaciers, characterized by a sudden onset of fast movement in usually slow-moving ice; quasiperiodic occurrence of phases of fast movement.

In the simplest case, a fast-moving ice stream is an autonomous system, that is, the movement is independent in time (constant velocity, standing crevasse patterns, time-independent dynamic parameters) (case A1). The simplest case in a surge is to consider one deformation event that affects previously undeformed ice (B1). (B1) is the case that lends itself most easily to mathematical treatment using displacement equations and strain matrices. (A1) is the case that is most easily treated if differential equations are employed.

(A1) autonomous system,

(B1) one deformation event.

The next levels of complication are

(B2) sequences of events as recorded by multiphase crevasse patterns,

(A2) time-dependent dynamic processes resulting in crevasse patterns.

Ramsay and Lisle (2000) use the term "heterogeneous patterns", not multiphase patterns, in rock structures to indicate several past deformation stages.

3 Prototypes of fast-moving ice deformation and data

Jakobshavns Isbræ is a prototype of a continuously fast-moving glacier. Jakobshavns Isbræ is located in Western Greenland at 69°N latitude, it accelerates to approximately 7 km/yr at the calving front and can be traced back over a distance of 80 km up onto the Greenland Inland Ice. Since the velocity of Jakobshavns Isbræ does not change throughout the seasons (following Echelmeyer and Harrison, 1990), it is an autonomous system (Mayer

and Herzfeld, 2000) and thus also a prototype for (A1). As part of a larger project on Jakobshavns Isbræ, we collected data of the following scales of resolution: Synthetic Aperture Radar (SAR) data from the European Space Agency's ERS-1 and ERS-2 satellites (resolution 12.5 m), aerial videographic data and GPS-referenced airphotos (submeter resolution), and ground-based Glacier Roughness Sensor (GRS) data (0.1 m horizontal resolution, subcentimeter vertical accuracy) (see Herzfeld et al., 1999).

Bering Glacier, Alaska, is a prototype of a surge glacier. The latest surge occurred in 1993-1995 (Herzfeld and Mayer, 1997; Herzfeld, 1998; Mayer and Herzfeld, 2000). During a surge, several deformation events or phases occur. After one deformation event, the glacier (or part of it) represents a prototype of (B1), after several events it is a prototype of (B2). In the three seasons of 1993-1995, we conducted field work and aerial observations on Bering Glacier and Bagley Ice Field. Video images and photographs from the onset of the surge provide material to study deformation events of class (B1) – clear-cut crevasses with sharp edges that occurred suddenly in otherwise undeformed ice with a slight snow cover. As the surge progressed, it extended downglacier and upglacier, affecting other areas and repeatedly affecting the same areas (surge waves, several individual events) (B2) (cf. Fig. 1).

4 Linear algebra background

Eigenvalue Theory. We assume the reader is familiar with eigenvalue theory and decompositions of matrices (see, e.g., Strang, 1988).

Theorem 1 (Singular value decomposition; SVD). A matrix $A \in I\!R^{(m,n)}$ has a decomposition, termed singular value decomposition

$$A = Q_1 \Sigma Q_2^{\mathrm{T}} \tag{1}$$

with the following properties:

(i) $Q_1 \in I\!R^{(m,m)}$ is an orthogonal matrix, the columns of Q_1 are eigenvectors of AA^{T};

(ii) $Q_2 \in I\!R^{(n,n)}$ is an orthogonal matrix, the columns of Q_2 are eigenvectors of $A^{\mathrm{T}}A$;

(iii) $\sqrt{\lambda_1}, \ldots, \sqrt{\lambda_r}$ singular values $\Sigma \in I\!R^{(m,n)}$ contains r with $r \leq \min(m,n)$ along the diagonal of the (r,r) upper left submatrix, where $\lambda_1, \ldots, \lambda_r$ are the nonzero eigenvalues of both AA^{T} and $A^{\mathrm{T}}A$ and r is the rank of both AA^{T} and $A^{\mathrm{T}}A$.

Theorem 2 (Polar decomposition). Let $A \in I\!R^{(n,n)}$. Then A has a decomposition

$$A = QU = VQ \tag{2}$$

with Q orthonormal and U and V symmetric and positive semidefinite. If A is invertible then U, V are positive definite.

Notice $U^2 = A^{\mathrm{T}}A$ and $V^2 = AA^{\mathrm{T}}$ and $Q = AU^{-1}$ are useful relationships.

Remark 1. The matrices Q and U in the polar decomposition are related to the singular value decomposition as follows:

$$A = Q_1 \Sigma Q_2^{\mathrm{T}} = Q_1 (Q_2^{\mathrm{T}} Q_2) \Sigma Q_2^{\mathrm{T}} = (Q_1 Q_2^{\mathrm{T}})(Q_2 \Sigma Q_2^{\mathrm{T}}) = QU.$$

Remark 2. The matrices Q_1, Q_2 in Theorem 1 (SVD) can be chosen such that they have norm one. Then the norm of Q is also equal to one, and Q defines a rotation in the unit sphere. In $I\!R^2$, we assume a right-hand coordinate system with counterclockwise rotation angles positive. As a rotation matrix in the unit circle, Q has the form

$$Q = \begin{pmatrix} \cos\alpha & -\sin\alpha \\ \sin\alpha & \cos\alpha \end{pmatrix},$$

where α is the angle of the rotation defined by Q. Given Q, the angle α is well-defined modulo 2π. (Notice that clockwise rotation is given by a negative angle α.)

5 Invariant analysis of the deformation gradient matrix

5.1 The deformation gradient matrix

Consider deformation in the horizontal plane within a homogeneous zone, and let (x, y) denote the original position of a point within the zone, and $(\hat{x}, \hat{y})$ the position after deformation. Deformation is described by a continuous function

$$\begin{aligned} &F(x,y) = (F_1(x,y),\ F_2(x,y)) = (F_1,\ F_2) \\ &\text{such that} \quad \hat{x} = F_1(x,y) \quad \text{and} \quad \hat{y} = F_2(x,y). \end{aligned} \tag{3}$$

The Jakobi matrix of F is termed (e.g., Liu, 2002) the *deformation gradient matrix*

$$M = \begin{pmatrix} \frac{\partial F_1(x,y)}{\partial x} & \frac{\partial F_1(x,y)}{\partial y} \\ \frac{\partial F_2(x,y)}{\partial x} & \frac{\partial F_2(x,y)}{\partial y} \end{pmatrix}. \tag{4}$$

5.2 Invariants resultant from singular value decomposition

Invariants of the deformation gradient matrix are useful to characterize and discriminate deformation types. First, we derive the invariants that are utilized in Ramsay and Lisle (2000). Using linear algebra, it can be shown that they are derived from the singular value decomposition, i.e. the eigenvalue analysis of the left Cauchy-Green tensor $B = V^2 = MM^{\mathrm{T}}$, the product of the deformation gradient matrix and its transpose (not from the eigenvalue analysis of M). B is a positive-definite and symmetric matrix, so (1) the singular value decomposition applies (Theorem 1), and (2) B is diagonalizable with eigenvalues λ_1 and λ_2.

Invariants of MM^{T} are

$$I_1 = \left(\frac{\partial F_1}{\partial x}\right)^2 + \left(\frac{\partial F_1}{\partial y}\right)^2 + \left(\frac{\partial F_2}{\partial x}\right)^2 + \left(\frac{\partial F_2}{\partial y}\right)^2, \tag{5}$$

$$I_2 = \frac{\partial F_1}{\partial x}\frac{\partial F_2}{\partial y} - \frac{\partial F_1}{\partial y}\frac{\partial F_2}{\partial x}. \tag{6}$$

The invariants are coefficients in the characteristic polynomial f_B, in particular $I_1 = \mathrm{tr}\,(B)$, the trace, and $I_2^2 = \det(B) = (\det M)^2$, and $I_2 = \det(M)$, the determinant. The eigenvalues λ_1 and λ_2 of B can be expressed in terms of the invariants:

$$\lambda_1 = \tfrac{1}{2}(I_1 + (I_1^2 - 4I_2^2)^{1/2}) \tag{7}$$

and

$$\lambda_1 = \tfrac{1}{2}(I_1 - (I_1^2 - 4I_2^2)^{1/2}). \tag{8}$$

5.3 Invariants from eigenvalue analysis

We also use the eigenvectors and eigenvalues of the deformation matrix M to describe deformation. Notice that not every matrix is diagonalizable and that cases with only one one-dimensional eigenspace exist in $\mathbb{R}^2$.

5.4 Rotation invariants

Using the polar decomposition, a deformation M can be interpreted geometrically as a rotation and an extension via $M = QU = VQ$, where $C = U^2 = M^{\mathrm{T}}M$ and $B = V^2 = MM^{\mathrm{T}}$ are the right and left Cauchy-Green tensors, respectively, and $Q = MU^{-1} = V^{-1}M$ is the rotation tensor. So, the right and left Cauchy-Green tensors of continuum mechanics (see, e.g., Liu, 2002) coincide with the major and minor products of the deformation matrix in factor analysis. Notice that M does not need to be symmetric or positive definite in general! A strain is called irrotational if $Q = E$, the identity matrix, which is equivalent to $M = U = V$ being symmetric and positive definite.

5.5 The inverse and the forward problem (the reciprocity of the structural-geology approach)

The deformation gradient matrix M, as defined above, is also known as the *deformation gradient matrix in Lagrangian form*, and denoted M_L for clarification. This is the solution to the forward problem. The solution to the inverse problem is termed *deformation gradient matrix in Eulerian form*, denoted M_E (where $M_E = M_L^{-1}$). Ramsay and Lisle (2000) use the terminology "displacement gradient matrix" for M_L and M_E. But, because displacement is defined as $u = (\hat{x}, \hat{y}) - (x, y)$, there is a difference between the deformation gradients M_L, M_E and the *displacement gradients* H_L, H_E, namely $M_L = 1 + H_L$ and $M_E = 1 - H_E$. The inverse exists only if $\det(M)$ is not zero, but $\det(M) > 0$ is guaranteed due to mass-conserving continuous motion evolving from the initial state with $M_L = M_E = 1$. Geologists commonly analyze deformed rocks and try to reconstruct the undeformed state, hence the whole approach is applied to M_E (not M_L) (see strain ellipses in Fig. 2).

According to the Singular value decomposition theorem, any positive-definite matrix A has a decomposition

$$A = Q\Lambda Q^{\mathrm{T}}$$

with $\lambda_i > 0$ for all i, with Q orthogonal and Λ diagonal. The rotation $y = Q^{\mathrm{T}}x$ simplifies $x^{\mathrm{T}}Ax = 1$ to $y^{\mathrm{T}}\Lambda y = 1$, or, $\sum_{i=1}^{n} \lambda_i y_i^2 = 1$ which describes an ellipsoid with axes of $1/\sqrt{\lambda_i}$ for $i = 1, \ldots, n$, and in the original x-space the axes point along the eigenvectors. In 2D, this ellipse has the *minor axis* in the direction of the *larger* eigenvalue's eigenvector and the *major axis* in the direction of the *smaller* eigenvalue's eigenvector (see Fig. 3).

The geologist is interested in the strain ellipsoid that shows the deformation and elongation. The major axis points in the direction of the *larger* eigenvalue's eigenvector and the length is equal to the eigenvalue. This explains why geologists (see Ramsay and Lisle,

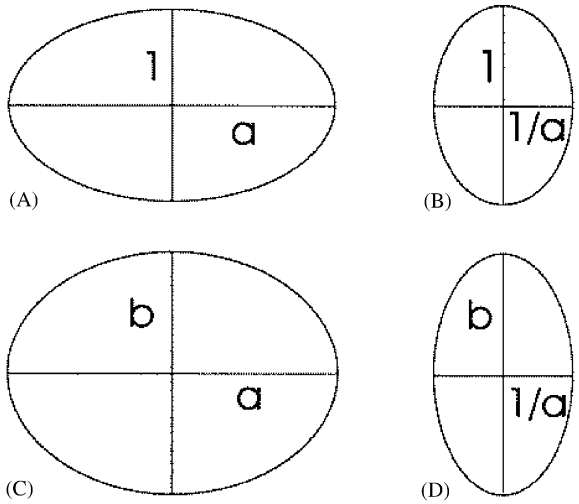

Figure 2: Strain ellipses corresponding to deformation gradient matrices for several cases: (A) extension in one direction; (B) compression in one direction; (C) extension in two orthogonal directions; (D) compression in one direction and extension normal to it.

2000) use the analysis of the reciprocal problem M_E, solve for the eigenvectors and eigenvalues of $C^{-1} = M_E M_E^{\mathrm{T}}$ (where $C = U^2 = M_L^{\mathrm{T}} M_L = M_E^{-\mathrm{T}} M_E^{-1} = (M_E M_E^{\mathrm{T}})^{-1}$ is the right Cauchy-Green tensor), obtain the "reciprocal quadratic principal finite strains" and then use the relationship $\lambda_i' = 1/\lambda_i$ to get the strain ellipsoid. A more direct approach is to decompose the left Cauchy-Green tensor $B = M_L M_L^{\mathrm{T}}$ and get the values λ_i directly, or to use the polar decomposition of M_L.

6 Relationship to connectionist-geostatistical ice-surface classification

Now how does an algebraic characterization of deformation matrices apply to the analysis of ice-surface types from fast-moving glaciers?

From video scenes or aerial photographs of the ice surface after deformation, prototypes of ice-surface classes may be derived. For the example of surging ice from the Bering Glacier surge 1993-1995, the classes are given in Fig. 1. Each image represents a type of deformation that we will analyze here using the algebra outlined in previous sections. As in structural geology, one image is sufficient for identification of the deformation type (unless too many deformation events have affected the ice surface, and too complex or chaotic crevassing has resulted). This is an advantage over methods geared at derivation of velocity information, which need two consecutive images or observations of the same area, and are restricted to simple types of movement, mostly linear or linearized ones.

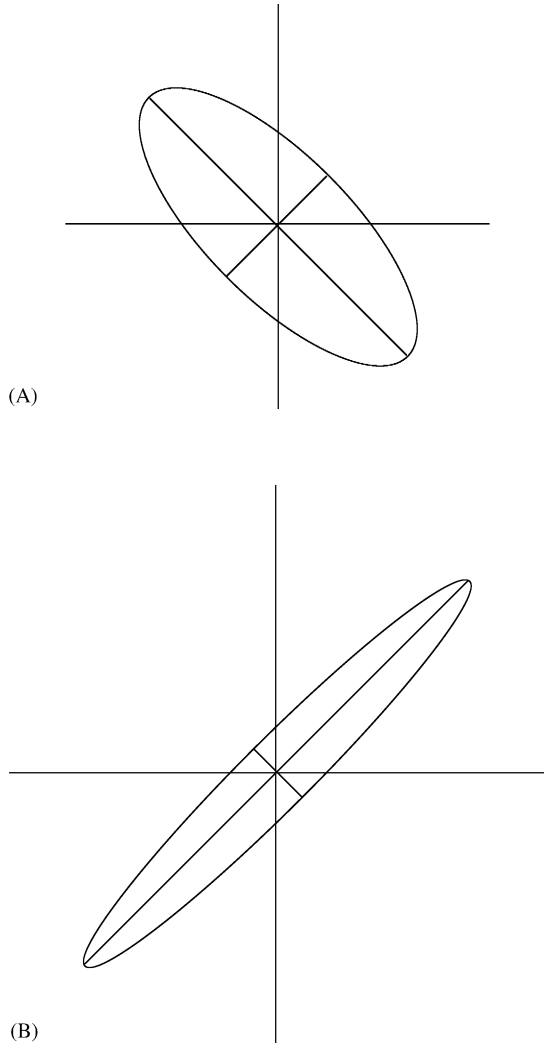

Figure 3: Example to reciprocal approach. $A = \begin{pmatrix} 5 & 4 \\ 4 & 5 \end{pmatrix}$: (A) ellipse with axes of $1/\sqrt{\lambda_i}$ for $i = 1, 2$, using notation as in Section 5.5. Minor axis points in direction of larger eigenvalue's ($\lambda_1 = 9$) eigenvector $v_1 = \begin{pmatrix} 1 \\ 1 \end{pmatrix}$, vector of minor axis is $\hat{v}_1 = \frac{1}{3} \begin{pmatrix} \frac{1}{\sqrt{2}} \\ \frac{1}{\sqrt{2}} \end{pmatrix}$, and major axis points in direction of smaller eigenvalue's ($\lambda_2 = 1$) eigenvector $v_2 = \begin{pmatrix} 1 \\ -1 \end{pmatrix}$, vector of the major axis is $\hat{v}_2 = \begin{pmatrix} \frac{1}{\sqrt{2}} \\ \frac{-1}{\sqrt{2}} \end{pmatrix}$; (B) strain ellipse. Major axis $\tilde{v}_1 = 9 \begin{pmatrix} \frac{1}{\sqrt{2}} \\ \frac{1}{\sqrt{2}} \end{pmatrix}$ points in direction of larger eigenvalue's eigenvector and length is equal to eigenvalue $\lambda_1 = 9$. Minor axis $\tilde{v}_2 = \begin{pmatrix} \frac{1}{\sqrt{2}} \\ \frac{-1}{\sqrt{2}} \end{pmatrix}$ points in direction of smaller eigenvalue's eigenvector and length is equal to eigenvalue $\lambda_2 = 1$.

Crevasse classes were determined using structural glaciology, and then applied to classify surge-type surfaces in the connectionist-geostatistical classification system (Herzfeld and Zahner, 2001). From a large number of images and replicates (100,000s) of ice surfaces, geostatistical functions and parameters are calculated, then a neural network is trained on the functions and parameters in a supervised form based on the established ice surface classes. Our approach facilitates analysis of more complex deformation events or processes, including deformation in several steps. If many deformation events have affected the ice surface such that the effects of individual events are no longer discernable, by eye or computer, then the deformation type is summarized as "complex" (chaos class). The final connectionist-geostatistical NNCLASS system is able to associate images of surge-type ice surfaces to ice surface classes, and hence to deformation states, 95% correctly for images previously unknown to the system.

Thus, we provide a link between a physical analysis of ice-surface deformation and a connectionist-geostatistical analysis of the same problem.

7 Application to crevasse pattern analysis

7.1 Crevasse patterns and deformation matrices for surge-type ice classes (B1 – one deformation event)

7.1.1 Undisturbed surface, chaos, and rest classes

Class 0 in Fig. 1 is a rest class in the automated method. Surfaces may show no crevasses and include rock or bare soil areas. The undeformed ice is, of course, described by the identity matrix as a deformation matrix. However, in an automated system, such as the connectionist-geostatistical classification system NNCLASS, each surface image that may be observed also needs to be classifiable; hence classes that cannot be described analytically need to be included in a rest class for completeness. While *class 1* contains images with, albeit complex, deformation patterns (see (7.4)), other images fall in *class 0*.

7.1.2 Extension in one direction

Class 2: Parallel crevasses and *class 3: Parallel crevasses with snow* (Fig. 1) which need to be discriminated in automated image analysis, are resultant of the same deformation type, extension in one direction (cf. Fig. 2A). The deformation gradient matrix is

$$M_L = \begin{pmatrix} a & 0 \\ 0 & 1 \end{pmatrix}, \quad a > 1. \tag{9}$$

Eigenvalues of M_L are a and 1, write $\sigma(M_L) = \{a, 1\}$ for the spectrum of A (the set of eigenvectors of M_L). Eigenvalues of

$$B = M_L M_L^{\mathrm{T}} = \begin{pmatrix} a^2 & 0 \\ 0 & 1 \end{pmatrix} \tag{10}$$

are a^2, 1.

7.1.3 Extension in two directions (see Fig. 1 class 5, class 6; Fig. 2 C)

The simplest two-dimensional pattern is extension in two directions. Bidirectional crevasses with one dominant direction ($a > b$) are exemplified in *class 5* of the surge-type crevasses (Fig. 1). The relative sizes of a and b are related to the extensional forces along the two axes. The most typical crevasse type in a surging glacier is *class 6: Square-top blocky crevasses* with $a \approx b$; its occurrence in fields in between undisturbed surface indicated the onset of a surge in Bering Glacier in June 1993 (Herzfeld, 1998; Lingle et al., 1993). The edges are clear-cut and disturb a fresh snow cover on the ice (if present), consequently the opening in both directions occurred at the same time (one deformation event). The difference between the ice surface patterns in *classes 5* and *6* demonstrates that not only the type of the matrix but also the relative size of the eigenvalues a, b is relevant in a classification.

In Jordan form, the matrix is

$$M_L = \begin{pmatrix} a & 0 \\ 0 & b \end{pmatrix}, \quad a, b > 1. \tag{11}$$

Eigenvalues of M_L are given by $\sigma(M_L) = \{a, b\}$. Eigenvalues of

$$B = M_L M_L^{\mathrm{T}} = \begin{pmatrix} a^2 & 0 \\ 0 & b^2 \end{pmatrix} \tag{12}$$

are given by $\sigma(B) = \{a^2, b^2\}$.

Invariants are

$$I_1 = a^2 + b^2, \quad I_2^2 = \det(B) = a^2 b^2, \quad I_2 = ab, \quad \mathrm{tr}\,(M_L) = a + b. \tag{13}$$

7.1.4 Two-directional extension under oblique angle

Acute-angle bidirectional crevasse patterns (*class 4*; Fig. 1) are similar to parallel crevasses, but deformational forces act in two directions. This may be caused by extensional forces in

two directions. Crevasses of the same age open in both directions orthogonal to them, as opposed to en-échelon crevasses which result from two deformation events (see 7.3). In the case of *class 4*, the extensional forces act along two directions with a large angle resulting in crevasses with a small angle (in the image in Fig. 1, the angle is approximately 15°), described by

$$M_L = T^{-1} \begin{pmatrix} a & 0 \\ 0 & b \end{pmatrix} T, \quad a, b > 1, \tag{14}$$

where T is a transformation matrix from the canonical basis to a basis with vectors v_1, v_2 forming a small angle, i.e. $T = (v_1, v_2)$ with respect to the canonical basis.

The rhombic pattern *class 7* is algebraically the same, but the angle of the basis vectors is approximately 45°. Thus the angular invariants serve as discriminants between *class 4* and *class 7*.

More specifically, the matrix has the following form: If two forces are acting under oblique angle, we may assume without loss of generality that the direction of the first force is $\begin{pmatrix} 1 \\ 0 \end{pmatrix}$ and the direction of the second force is $\begin{pmatrix} c \\ s \end{pmatrix} = \begin{pmatrix} \cos\alpha \\ \sin\alpha \end{pmatrix}$ with $s \neq 0$ since $\alpha \neq 0$. Both are eigenvectors for some eigenvalues a, b which are magnitudes of the extensional forces:

$$M_L \begin{pmatrix} 1 \\ 0 \end{pmatrix} = a \begin{pmatrix} 1 \\ 0 \end{pmatrix} \quad \text{and} \quad M_L \begin{pmatrix} c \\ s \end{pmatrix} = b \begin{pmatrix} c \\ s \end{pmatrix}. \tag{15}$$

It follows

$$M_L = \begin{pmatrix} a & \frac{(b-a)c}{s} \\ 0 & b \end{pmatrix}. \tag{16}$$

Let us assume $b \neq a$. $\sigma(M_L) = \{a, b\}$, the characteristic polynomial is $f_{M_L} = (\lambda - a)(\lambda - b)$, the trace is $\mathrm{tr}\,(M_L) = a + b$, and since $a \neq b$, the first invariant provides a discriminator between oblique-angle two-directional extension and orthogonal two-directional extension (7.1.3).

If $b = a$, then we have

$$M_L = \begin{pmatrix} a & 0 \\ 0 & a \end{pmatrix},$$

the case of square-top blocky crevasses (see 7.1.3).

7.2 Examples of compression and extension-compression (B1)

7.2.1 Compression in one direction (see Fig. 2B)

Compression in one direction can lead to (1) compression fractures (reverse faults and thrusts with shortening and thickening – orientation normal to compressional force), (2) conjugate shear faults oblique to compressional force with shortening and widening, (3) opening of parallel crevasses in the direction parallel to the direction of the compressional force with shortening and widening. Here, we consider case (1):

The matrix describing a compressional force only is

$$M_L = \begin{pmatrix} \frac{1}{a} & 0 \\ 0 & 1 \end{pmatrix}, \quad a > 1. \tag{17}$$

Eigenvalues of M_L are $1/a$ and 1. Eigenvalues of

$$B = M_L M_L^{\mathrm{T}} = \begin{pmatrix} \frac{1}{a^2} & 0 \\ 0 & 1 \end{pmatrix} \tag{18}$$

are $1/a^2$, 1.

7.2.2 Extension-compression (see Fig. 2D)

Now we consider case (3) mentioned in Section 7.2.1: If crevasses open that means the ice follows extensional movement in the direction normal to the compressional force. Consequently, the matrix describing a compressional force only is

$$M_L = \begin{pmatrix} \frac{1}{a} & 0 \\ 0 & b \end{pmatrix}, \quad a, b > 1. \tag{19}$$

Eigenvalues of M_L are $1/a$ and b. Eigenvalues of

$$B = M_L M_L^{\mathrm{T}} = \begin{pmatrix} \frac{1}{a^2} & 0 \\ 0 & b^2 \end{pmatrix} \tag{20}$$

are $1/a^2$, b^2.

Invariants:

$$I_1 = \frac{1}{a^2} + b^2, \quad I_2^2 = \det(B) = \frac{b^2}{a^2}, \quad I_2 = \frac{b}{a}, \quad \mathrm{tr}\,(M_L) = \frac{1}{a} + b. \tag{21}$$

Examples of compression or extension-compression are found in crevasses forming where

ice flows against an obstacle such as a mountainside.

7.3 An example of several deformation events in surging ice (B2)

All of the previously given examples (except for those in 7.1.1) fall in the class of crevasse patterns caused by a single deformation event. The extensional types occur as surge crevasses, whereas the compressional types or mixtures may occur in constrictions. The observation that most surge crevasses are of the extensional type matches what is known about the theory of glacier surges (cf. Herzfeld, 1998). Compressional forms and mixed forms may occur when the initial surge crevasses are transported and transformed by subsequent deformation events. In the analysis of multiple deformation events, we utilize crosscutting and overprinting relationships of structural features to deduce the sequence of events, as is common practice in structural geology.

The example of en-échelon crevasses, which have been observed in Bering Glacier and Bagley Ice Field during the surge and are represented as *class 8* (Fig. 1) is an example of two deformation events acting on the ice at two different times. En-échelon crevasses open also when ice during the relaxation in upper areas of a surge extends, then is transported across areas where crevasses may be induced by subglacial topography (examples of Bagley Ice Field, Alaska, during the end of the Bering Glacier surge in 1995 are given in Herzfeld and Mayer, 1997; Herzfeld, 1998).

First, extension occurred in one direction; later, extension occurred in a different direction, and the extensional forces of the second event are broken (deflected) at the weaknesses caused by the first deformation event, this causes the typical "tails" along the edges of the first-generation crevasses. So, the second deformation acts on a coordinate system that is rotated relative to the first one, i.e.

$$M_L = R^{-1} \begin{pmatrix} b & 0 \\ 0 & 1 \end{pmatrix} R \begin{pmatrix} a & 0 \\ 0 & 1 \end{pmatrix}, \quad a, b > 1, \tag{22}$$

where the last matrix marks the first event, and the other three mark the second event; and

$$R = \begin{pmatrix} \cos\alpha & -\sin\alpha \\ \sin\alpha & \cos\alpha \end{pmatrix} \tag{23}$$

is the basis transformation matrix of a rotation of angle α.

7.4 Complex deformations

The ice surface in *class 1: Chaos* (Fig. 1) is a result of a complicated superposition of many deformation events, which are too complex to be reconstructed individually.

The algebraic part describes and formalizes the forward problem of crevasse formation in sequential steps. The deformation steps result in a deformation pattern that is visible as crevasse pattern in the ice surface. Because of mass conservation, the inverse problem can also be solved – deformation is deduced from observed crevasse patterns, for every deformation event. In the inverse problem, however, steps of the deformation need to be reconstructed, similar to the problem of reconstructing deformation in geology (but specific to the properties of the rock, the material ice, which permits both ductile and brittle deformation). Usually, the sequence of deformation events may be reconstructed using crosscutting and overprinting relationships for a number n of events, for a small integer n. After a number of steps, not only is it impossible to imagine the precise deformation events, but it is also not meaningful to study the events that lead to a completely broken-up ice surface of standing and fallen seracs and crushed pieces of ice (see, e.g., the image in Fig. 1, class 1). Hence, it is sensible to summarize complex patterns into one class, termed "chaos" (class 1 here), which provides a clean solution of the classification problem.

8 The problem of shear – application to margins of fast-moving ice streams

In aerial photographs or high-resolution satellite images, a fast-moving ice stream is most easily recognized by its heavily crevassed, wide shear margins which result from the fast flow of the central ice stream through the surrounding slow-moving ice. The shear margin is characterized by a large rotational component. In existing glaciological models, large rotational components are rarely taken into account; in geology, to the contrary, large rotational components are frequently observed and treated (see, e.g., Ramsay and Lisle, 2000). In the case of the fast-moving ice stream, different flow equations govern the fast-moving part and the slow-moving part. The fast-moving ice, the margins, and the slow-moving ice together are not a single continuous unit in the sense of classical continuum mechanics. A solution lies in the introduction of damage as a scalar parameter dependent on across-flow distance (simpler), or as a tensorial variable (better); then margin, ice stream and slow ice may be treated as a unit in the sense of continuum damage mechanics (see Clarke and Herzfeld (2000); this will be treated in a different paper).

As an example, we analyze a crevasse type from Jakobshavns Isbræ, West Greenland (Fig. 4). At the margin of the ice stream, shear crevasses occur. The shear margin

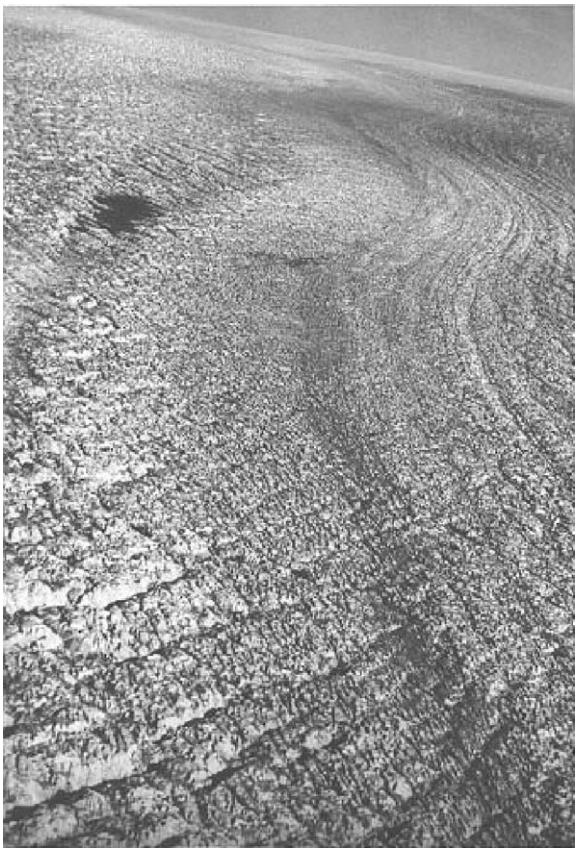

Figure 4: Shear margin of Jakobshavns Isbræ, West Greenland. Dominant crevasses in foreground are shear crevasses. Center of ice stream is to right. View is east, upglacier.

between the fast-moving ice stream, which accelerates to 7 km/yr at the calving front (Echelmeyer et al., 1991; Pelto et al., 1989), and the slow-moving Greenland Inland Ice (velocity 0.3 m/yr according to our GPS measurements) is several kilometers wide (Mayer and Herzfeld, 2001). The ice stream together with the inland ice cannot be considered a continuum any more because of the high degree of fracturing.

The shear matrix

$$M_L = \begin{pmatrix} a & 1 \\ 0 & a \end{pmatrix} \tag{24}$$

is not symmetric and not diagonalizable. The only eigenvalue is $\sigma(M_L) = a$, the related eigenspace is one dimensional, and the geometric multiplicity of the eigenvalue is one, but its algebraic multiplicity is two. Along direction $\begin{pmatrix} 1 \\ 0 \end{pmatrix}$ (eigenvector) there is an extension by a factor of a.

8.1 Simple shear

The deformation matrix of simple shear is

$$M_L = \begin{pmatrix} 1 & y \\ 0 & 1 \end{pmatrix} \tag{25}$$

with $y \neq 0$. The only eigenvalue is 1, associated with a one-dimensional eigenspace.

8.2 Shear with extension

The more complex situation of shear with extension may be considered a (B2)-type deformation, or a one-step complex deformation. Multiplication of the matrices of extension and simple shear yields

$$\begin{pmatrix} a & 0 \\ 0 & a \end{pmatrix} \begin{pmatrix} 1 & y \\ 0 & 1 \end{pmatrix} = \begin{pmatrix} a & ay \\ 0 & a \end{pmatrix} \tag{26}$$

so with $\hat{y} = ay$ the general form is

$$M_L = \begin{pmatrix} a & \hat{y} \\ 0 & a \end{pmatrix}. \tag{27}$$

Eigenvector analysis leads to $\sigma(M_L) = \{a\}$, algebraic multiplicity is 2 and geometric multiplicity is 1. The only eigenvector is $\begin{pmatrix} 1 \\ 0 \end{pmatrix}$; $\mathrm{tr}\,(M_L) = 2a$ and $\det(M_L) = a^2$. Analysis of the characteristic polynomial f_B yields

$$\lambda_{1,2} = \frac{2a^2 + \hat{y}^2}{2} \pm \sqrt{\frac{\hat{y}^4}{4} + a^2\hat{y}^2}$$

and $\sqrt{\lambda_1} = \sigma_1$, $\sqrt{\lambda_2} = \sigma_2$ are the invariants in Eqs. (7) and (8). For instance, for

$$M_L = \begin{pmatrix} 1 & 2 \\ 0 & 1 \end{pmatrix}, \quad \sigma_1 = 2.41 \quad \text{and} \quad \sigma_2 = 0.41.$$

9 Discussion and conclusions

The presented work provides the mathematical description of the geometrical component of a new method for the analysis of ice deformation. Our analysis results in a classification of crevasse types which are (1) associated with deformation and thus provide information on ice dynamics, and (2) are described by quantitative parameters with bounds and relative sizes (such as $a > b > 1$) but not by numerical values (such as $a = 5.372$, $b = 2.489$) except

for examples. In combination with the connectionist-geostatistical method, it is a tool for fast and efficient geophysical analysis of ice dynamics from satellite or aerial photographic imagery.

A simplification in the present approach is the reduction from three- to two-dimensional analysis. This reduction is done, because only a two-dimensional part is visible in the ice surface. The maximal dimension of any rotation in $\mathbb{R}^3$ is two, with the third dimension being the rotation axis. Algebraically, the rotation axis is not necessarily one of the three basis directions (longitudinal, transverse to ice flow, and vertical), so it could be oblique to the ice surface and consequently, the basis transformation that is necessary to present the matrix in the decomposition form

$$\begin{pmatrix} R & 0 \\ 0 & 1 \end{pmatrix},$$

where R is a rotation matrix as in Eq. (23), and the 0's are two-dimensional vectors, would change the submatrix R. In reality, however, crevasse-forming rotational components in the ice occur with the rotation axis vertical or close to vertical to the ice surface. Therefore, $R \approx \tilde{R}$, denoting by $\tilde{R}$ the rotation matrix associated with the observed crevasse pattern and by R the rotation matrix associated with basis transformation such that the three-dimensional deformation matrix has canonical form

$$\begin{pmatrix} R & 0 \\ 0 & 1 \end{pmatrix}.$$

Hence, the matrix R derived from a two-dimensional analysis is close to the projection of the three-dimensional matrix into $\mathbb{R}^2$.

For instance, shear along a glacier margin has a near-vertical axis of the rotation component, the axis may be inclined caused by the geometry of the valley, and shear of an ice stream flowing fast in slow-moving adjacent ice has a vertical rotation axis. Basal shear (shear of the flowing ice against the bedrock) usually does not create crevasses in the ice surface because of the viscosity of the material ice and the thickness of glaciers (except in the area very close to the glacier's snout). A similar argument holds for the extensional or compressional component (U, V in polar decomposition). There, it is easier, because U, V are symmetric and thus diagonalizable.

In conclusion, results of a two-dimensional analysis are a good approximation of the three-dimensional deformation in the case of crevasse-pattern analysis.

Consideration of the appropriate scale is essential to the study of crevasses. From laboratory experiments on the physics of ice, one may conclude that ice always cracks

at certain angles which are induced by the crystal structure. On the scale of crevasses, however, the rules of structural geology apply; fast-moving ice behaves like rock under brittle deformation. As a footnote, we remark that ice surface structure is not self-similar (but possibly fractal), as it has different behavior at small and large scale.

Observation demonstrates that crevasses of different angles occur (e.g., Fig. 1 classes 4 and 7). In particular, we note that in reality two forces acting under an oblique angle do not result in a rectangular crevasse field with axes corresponding to those of the strain ellipsoid, but cause different patterns depending on angle and discernable by the first invariant.

10 Outlook

Several factors that may contribute to crevasse patterns have not been treated here. Transport of ice downglacier affects the location and appearance of crevasses. Changes in orientation may occur, or crevasses may close in an area of compression. Mathematically, a basis transformation acts on the coordinate axes of the system, and the time aspect needs to be modeled.

The treatment here concerns the structural aspect of the deformation and the resulting pattern of crevasses. However, it is a question of material properties to establish how many crevasses may actually open per unit length or area under a given deformation type. Continuum damage mechanics (Krajcinovic, 1996) provides an avenue for analysis in a stochastic mechanics framework, which utilizes probability density functions from which crack density may be inferred (Clarke and Herzfeld, 2000). The density of crevasses must depend on the extensional force, for instance, if $a > b > 1$ in the matrices of one-dimensional extension

$$\begin{pmatrix} a & 0 \\ 0 & 1 \end{pmatrix} \quad \text{and} \quad \begin{pmatrix} b & 0 \\ 0 & 1 \end{pmatrix}$$

(cf. Eq. (11)), then more crevasses or wider crevasses or larger crevasses should form. Whether a larger extensional force causes more (small) OR (the same number of) larger crevasses may also depend on ice temperature or viscosity/plasticity, crystal structure and density (age of the ice), dust and sediment content and distribution, texture or fabric.

In structural geology, a similar question is not treated; but the relationship between the observed appearance of a rock that has undergone a certain deformation and the deformation type is clearly established in the literature. The deformation type then may be used to identify the deformation gradient matrix and subsequent analysis, as derived here.

Acknowledgements

Support by Deutsche Forschungsgemeinschaft under grants DFG He1547/7-1, He1547/9 (with use of data from projects DFG He1547/4 and He1547/8) to U.C. Herzfeld and DFG Ma2486/1-1 to H. Mayer is gratefully acknowledged, as is support for U.C. Herzfeld under the CIRES Visitor Fellowship.

References

Clarke, G.K.C., 1987. Fast glacier flow: ice streams, surging, and tidewater glaciers. Journal of Geophysical Research 92 (B9), 8835–8841.

Clarke, G.K.C., Herzfeld, U.C., 2000. An approach to modeling crevasse pattern formation. Eos Transactions American Geophysical Union 81 (48 Suppl.), F427.

Echelmeyer, K., Harrison, W.D., 1990. Jakobshavns Isbræ, West Greenland: seasonal variations in velocity – or lack thereof. Journal of Glaciology 36 (122), 82–88.

Echelmeyer, K., Clarke, T.S., Harrison, W.D., 1991. Surficial glaciology of Jakobshavns Isbræ, West Greenland: Part I. Surface morphology. Journal of Glaciology 37 (127), 368–382.

Herzfeld, U.C., 1998. The 1993-1995 surge of Bering Glacier (Alaska) – a photographic documentation of crevasse patterns and environmental changes . Trierer Geographische Studien 17, 211 pp.

Herzfeld, U.C., Mayer, H., 1997. Surge of Bering Glacier and Bagley Ice Field, Alaska: an update to August 1995 and an interpretation of brittle-deformation patterns. Journal of Glaciology 43 (145), 427–434.

Herzfeld, U.C., Zahner, O., 2001. A connectionist-geostatistical approach to automated image classification, applied to the analysis of crevasse patterns in surging ice. Computers & Geosciences 27 (5), 499–512.

Herzfeld, U.C., Mayer, H., Feller, W., Mimler, M., 1999. Glacier roughness surveys of Jakobshavns Isbræ Drainage Basin, West Greenland, and morphological characterization. Zeitschrift für Gletscherkunde und Glazialgeologie 35 (2), 117–146.

Krajcinovic, D., 1996. Damage mechanics. North-Holland Series in Applied Mathematics and Mechanics, Vol. 41. North-Holland (Elsevier), New York, 774 pp.

Lingle, C.S., Post, A., Herzfeld, U.C., Molnia, B.F., Krimmel, R.M., Roush, J.J., 1993. Bering Glacier surge and iceberg-calving mechanism at Vitus Lake, Alaska, USA. Journal of Glaciology 39 (133), 722–727.

Liu, I-S., 2002. Continuum Mechanics. Springer, Berlin, 297 pp.

Marmo, B.A., Wilson, C.J.L., 1998. Strain localisation and incremental deformation within ice masses, Framnes Mountains, east Antarctica. Journal of Structural Geology 20 (2/3), 149–162.

Marrett, R., Peacock, D.C.P., 1999. Strain and stress. Journal of Structural Geology 21 (8/9), 1057–1063.

Mayer, H., Herzfeld, U.C., 2000. Structural glaciology of the fast-moving Jakobshavn Isbræ, Greenland, compared to the surging Bering Glacier, Alaska, USA. Annals of Glaciology 30, 243–249.

Mayer, H., Herzfeld, U.C., 2001. A structural segmentation, kinematic analysis and dynamic interpretation of Jakobshavns Isbræ, West Greenland. Zeitschrift für Gletscherkunde und Glazialgeologie 37 (2), 107–123.

Means, W.D., 1976. Stress and Strain: Basic Concepts of Continuum Mechanics for Geologists. Springer, New York, NY, 339 pp.

Pelto, M.S., Hughes, T.J., Brecher, H.H., 1989. Equilibrium state of Jakobshavns Isbræ, West Greenland. Annals of Glaciology 12, 127–131.

Ramsay, J.G., Lisle, R.J., 2000. The Techniques of Modern Structural Geology, Vol. 3: Applications of Continuum Mechanics in Structural Geology. Academic Press, San Diego, CA, pp. 701–1061.

Rist, M.A., Sammonds, P.R., Murrell, S.A.F., Meredith, P.G., Doake, C.S.M., Oerter, H., Matsuki, K., 1999. Experimental and theoretical fracture mechanics applied to Antarctic ice feature and surface crevassing. Journal of Geophysical Research 104 (B2), 2973–2987.

Sanderson, D.J., 1982. Models of strain variation in nappes and thrust sheets; a review. In: Williams, G.D. (Ed.), Strain within Thrust Belts. Tectonophysics 88 (3–4), 201–233.

Şengör, A.M.C., 2002. What's wrong with shortening? GSA Today 12 (1), 31.

Strang, G. 1988. Linear Algebra and Its Applications, 3rd edition, Harcourt Brace Jovanovich Publishers, San Diego, CA, 505 pp.

Suppe, J., 1985. Principles of Structural Geology. Prentice-Hall, Englewood Cliffs, NJ, 537 pp.

Twiss, R.J., Moores, E.M., 1992. Structural Geology. W.H. Freeman, New York, NY, 532 pp.

Vornberger, P.L., Whillans, I.M., 1990. Crevasse deformation and examples from Ice Stream B, Antarctica. Journal of Glaciology 36 (122), 3–10.